Superparaelectric phase in the ensemble of noninteracting ferroelectric nanoparticles

M. D. Glinchuk, E. A. Eliseev, and A. N. Morozovska*
Institute for Problems of Materials Science, NAS of Ukraine, Krjijanovskogo 3, 03142 Kiev, Ukraine
(Received 20 June 2008; published 22 October 2008)

We predict the conditions of superparaelectric phase appearance in the ensemble of noninteracting spherical ferroelectric nanoparticles. The superparaelectricity in the ensemble of nanoparticles was defined by analogy with superparamagnetism, obtained earlier in small nanoparticles made of magnetic material. Calculations of correlation radius, energetic barriers of polarization reorientation, and polarization response to external electric field, performed within Landau-Ginzburg phenomenological approach for perovskites $Pb(Zr,Ti)O_3$, $BiFeO_3$, uniaxial ferroelectrics Rochelle salt, and triglycine sulfate, proved that under the favorable conditions ensemble of noninteracting nanoparticles possesses superparaelectric features. The main favorable conditions for the superparaelectricity observation in ferroelectric nanoparticles are the radius smaller than the correlation radius, surface screening of depolarization field, small Curie-Weiss constant, and high nonlinear coefficients, which guarantee that the barrier of the particle polarization orientation will be smaller than the thermal energy and the particle is single domain. The theoretical forecast is waiting for experimental revealing.

DOI: 10.1103/PhysRevB.78.134107 PACS number(s): 77.80.Fm, 77.22.Ej

I. INTRODUCTION

Ferroelectric, ferromagnetic, and ferroelastic materials belong to primary ferroics,[1] so that one can expect the similarity of their properties not only in bulk samples, but in nanomaterials also. One of the most interesting and broadly investigated phenomenon in ensemble of ferromagnetic noninteracting nanoparticles was shown to be superparamagnetic phase (see, e.g., Refs. 2 and 3 and references therein). This phenomenon is related to the fact that for nanoparticle with radius smaller than magnetic exchange length a barrier between different orientations of magnetization is of the order of k_BT at temperatures $T<100$ K because it is proportional to the nanoparticle volume. As a result, the particle can be considered as a free reorientable one up to some low enough blocking temperature T_b, smaller than the barrier height. At $T<T_b$ magnetic hysteresis loop appears, which is characteristic for monodomain ferromagnetic. Magnetization of the noninteracting nanoparticles in magnetic field has no quantization contrary to paramagnetic molecules. It can be described similarly to classic paramagnetics by Langevin function where the moment of whole particle and not the moment of separate ions has to be considered as elementary magnetic moment.[4] As a result the relaxation time of thermoactivated magnetization is much larger than for conventional paramagnetics.

One could expect the appearance of similar phase in the other primary ferroics, in particular in the ensemble of ferroelectric nanoparticles. Despite the technology progress in production of these systems, for instance, using porous matrices,[5–7] up to now nothing is known about superparaelectric phase in ensembles of ferroelectric nanoparticles; also the term "superparaelectric" was used for the description of bulk ferroelectric relaxors.[8–10] There were attempts to apply the term to ferroelectric film[11] and to the ferroelectric nanoparticles.[12,13] However the observed properties were characteristic mainly to paraelectric phase rather than to superparaelectric one.

In this paper we considered the conditions at which superparaelectric phase would exist in ferroelectric nanoparticles. In our approach we define superparaelectrics' characteristic features by analogy with those of superparamagnetics. First of all we took into account that while in magnetic nanoparticles exchange interaction tries to align magnetic moments of ions the correlation effect plays the same role in ferroelectric nanoparticles. Actually, polarization fluctuation correlations are determined by the correlation radius,[14] originated from the long-range interactions. Therefore in the nanopartcile with radius smaller than correlation radius all the electric dipoles have to be aligned in the same direction. So we arrive to the pattern of nanoparticles with large enough electric dipoles. The behavior of the ensemble of such noninteracting nanoparticles under the external electric field, temperature, and other factors has to define the size-dependent characteristic features of superparaelectric phase. Below we listed these features for the case of spherical ferroelectric nanoparticles.

(1) When the particle radius R is less than the correlation radius R_c, but higher than the critical radius R_{cr} of size-driven ferroelectric-paraelectric phase transition, all dipole moments inside the particle are aligned due to the correlation effects.

(2) Surface screening of depolarization field that makes the particle single-domain state energetically preferable.

(3) Potential barrier $\Delta F(T,R)$ of polarization reorientation can be smaller than thermal activation energy at temperatures T higher than the freezing temperature $T_f(R)$ depending on the particle radius R. Freezing temperature $T_f(R)$ can be estimated from the condition $\Delta F(T_f,R)=k_BT_f$. Such determination is somehow voluntary, since the rigorous value of $T_f(R)$ depends on numerical factor γ before k_BT, which depends on the system characteristics.

(4) Langevin-like law for polarization dependence on external field is obtained at temperatures higher than the freezing temperature $T_f(R)$, but lower than the temperature $T_{cr}(R)$ of size-driven ferroelectric-paraelectric phase transition.

(5) Ferroelectric hysteresis loop and remnant polarization appear at temperatures T lower than the freezing temperature $T_f(R)$. This behavior can be named as frozen superparaelectric phase.

The conditions (1)–(5) determine the superparaelectric phase appearance in the ensemble of ferroelectric nanoparticles of radius $R_{cr}<R<R_c$ at temperatures $T_f(R)<T<T_{cr}(R)$.

In Sec. II we performed calculations of correlation radius dependence on the particle radius, temperature, and ferroelectric material parameters. Potential barrier of polarization reorientation in ferroelectric nanoparticle is calculated in Sec. III. Polarization dependence on electric field and hysteresis loop calculations allowing for barrier existence are presented in Sec. IV. Superparaelectricity appearance in ferroelectric nanoparticles is discussed in Sec. V.

II. CORRELATION RADIUS DEPENDENCE ON PARTICLE RADIUS

Let us introduce a correlation function of polarization z-component $P_3(\mathbf{r})$ fluctuations in conventional way[15]

$$G(\mathbf{r},\mathbf{r}') = \langle [P_3(\mathbf{r}) - \langle P_3(\mathbf{r})\rangle][P_3(\mathbf{r}') - \langle P_3(\mathbf{r}')\rangle]\rangle, \quad (1)$$

where $\langle \ldots \rangle$ stands for thermal (statistical) averaging. Using the fluctuation-dissipation theorem,[14,16] one can rewrite the correlation function (1) via a generalized susceptibility $\chi(\mathbf{r},\mathbf{r}')$ in the form $G(\mathbf{r},\mathbf{r}')=k_BT\chi(\mathbf{r},\mathbf{r}')$, where $\chi(\mathbf{r},\mathbf{r}')$ determines the increment of polarization $\delta P_3(\mathbf{r})$ under the inhomogeneous electric field $\delta E_3(\mathbf{r}')$:

$$\delta P_3(\mathbf{r}) = \int \chi(\mathbf{r},\mathbf{r}')\,\delta E_3(\mathbf{r}')d\mathbf{r}'. \quad (2)$$

In order to find the generalized susceptibility $\chi(\mathbf{r},\mathbf{r}') \sim G(\mathbf{r},\mathbf{r}')$ of confined system, one has to consider the equation of state for z component of the polarization $P_3(\mathbf{r}) = P(\mathbf{r}) + \delta P_3(\mathbf{r})$:

$$a_1 P_3 + a_{11} P_3^3 - \zeta \frac{\partial^2 P_3}{\partial z^2} - \eta\left(\frac{\partial^2 P_3}{\partial x^2} + \frac{\partial^2 P_3}{\partial y^2}\right) = E_0 + E_d(P_3) + \delta E_3. \quad (3)$$

Gradient terms are $\zeta>0$ and $\eta>0$; expansion coefficient is $a_{11}>0$ for the second order phase transitions. Coefficient $a_1(T)=\alpha_T(T-T_c)$ and T_c is the transition temperature of bulk material. Note, that the coefficient a_{11} for displacement type ferroelectrics does not depend on T, while it is temperature dependent for order-disorder type ferroelectrics [see mathematical details in Appendix A of Ref. 17.

E_0 is the homogeneous external field, the term $E_d(P_3)$ represents depolarization field, that increases due to the polarization inhomogeneity in confined system. Linear operator $E_d(P_3)$ essentially depends on the system shape and boundary conditions at $E_d(0)\equiv 0$. For the most of the cases it has only integral representations, which reduces to constant (depolarization factors) only for special case of ellipsoidal bodies with homogeneous polarization distribution. In this case of polarization dependence on the x and y coordinates simple expression for electric depolarization field, obtained by Kretschmer and Binder,[18] is not valid. Below we consider the case when depolarization field is completely screened by the ambient free charges σ outside the dielectric particle (short circuit electrical boundary conditions), while it is nonzero, but small enough inside the dielectric particle due to inhomogeneous polarization distribution (i.e., nonzero div $\mathbf{P}\neq 0$) [see Fig. 1(b)]. Corresponding expression for the spherical particle depolarization field is derived in Appendix B of Ref. 17.

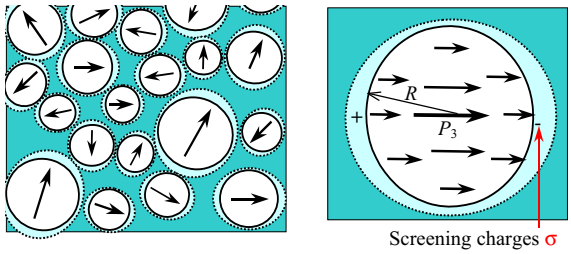

FIG. 1. (Color online) (a) Ensemble of noninteracting ferroelectric nanoparticles covered outside by the ambient free charges σ. All particle radii R are less than the correlation radius R_c, so that the dipole moments inside the particle are aligned due to the correlation effects. (b) A given nanoparticle, where the arrows inside the particle indicate the absolute value of dipole moments in different points.

Note that open circuit electrical boundary conditions for single ferroelectric nanoparticles of different shapes were considered by Naumov and co-workers[19–21] and Slutsker *et al.*[22] The various types of domain structures were found, including vortices.[19] However when the boundary conditions tend to short circuit, the nanoparticle becomes single domain.[20] Since only individual nanoparticles were considered in Refs. 19–22 the depolarization field outside the particles was ignored despite partial screening should lead to its appearance. Given that the depolarization field is responsible for electrostatic interaction between nanoparticles in the ensemble, the partial screening may lead to the formation of superstructures inside ensemble. Since we aim to consider the conditions of superparaelectric phase appearance, we restricted our model to the case of weak deviation from perfect screening case, when the field outside the particles is small and interaction between nanoparticles could be neglected.

The boundary conditions depend on the geometry and surface energy of the system depending on the extrapolation length λ.[28] For the spherical particle of radius R the boundary conditions are

$$\left(\lambda \frac{dP_3}{dr} + P_3\right)\Big|_{r=R} = 0, \quad (4)$$

where $r=\sqrt{x^2+y^2+z^2}$ is radius in spherical coordinates. The typical values are $|\lambda|=0.5-50$ nm.[23]

Using equation of state (3), one can write the linearized equation for the fluctuation δP_3 as

$$[a_1 + 3a_{11}P^2(\mathbf{r})]\delta P_3 + E_d(\delta P_3) - \zeta\frac{\partial^2 \delta P_3}{\partial z^2} - \eta\left(\frac{\partial^2 \delta P_3}{\partial x^2} + \frac{\partial^2 \delta P_3}{\partial y^2}\right) = \delta E_3. \quad (5a)$$

The equilibrium polarization $P\equiv P_3^0$ satisfies the nonlinear equation

$$a_1 P + a_{11} P^3 - \zeta \frac{\partial^2 P}{\partial z^2} - \eta \left(\frac{\partial^2 P}{\partial x^2} + \frac{\partial^2 P}{\partial y^2} \right) = E_0 + E_d(P). \tag{5b}$$

Maxwell's equations $\mathrm{div}\{\mathbf{P}(\mathbf{r}) + \varepsilon_0[\mathbf{E}_d(\mathbf{r}) + \mathbf{E}_0]\} = 0$ and $\mathrm{rot}\, \mathbf{E}_d(\mathbf{r}) = 0$ lead to the expression in Fourier $\mathbf{k}$ representation $\delta\tilde{\mathbf{E}}_d = -(\frac{\delta\tilde{\mathbf{P}}(\mathbf{k})}{\varepsilon_0}\mathbf{k}/k)\frac{k}{\mathbf{k}}$.[24] So, the relation between depolarization field fluctuations $\tilde{E}_d$ and polarization $\delta P_3(\mathbf{r})$ is

$$\tilde{E}_d = -\frac{k_3^2}{\varepsilon_0 k^2} \delta\tilde{P}_3(\mathbf{k}). \tag{6}$$

In Appendix B2 of Ref. 17 we had shown the validity of Eq. (6) for nanoparticles.

Using the definition of generalized susceptibility (2) and Eqs. (5) and (6), we obtained the approximate solution for linearized susceptibility $\tilde{\chi}(\mathbf{k}) \sim \tilde{G}(\mathbf{k})$ in Fourier $\mathbf{k}$ representation as

$$\tilde{\chi}(\mathbf{k}) \approx \frac{1}{3a_{11}\bar{P}^2 + a_R(T,R) + \eta(k_1^2 + k_2^2) + (\zeta + 1/\varepsilon_0 k^2)k_3^2}. \tag{7}$$

Equation (7) works well for low $\mathbf{k}$ values (long-wave approximation). $\bar{P}$ is the equilibrium polarization averaged over the nanoparticle volume which satisfies the equation $a_R(T,R)\bar{P} + a_{11}\bar{P}^3 = E_0$. At zero external field $E_0 = 0$, the spontaneous polarization is nonzero in ferroelectric phase, $\bar{P}^2 = -a_R(T,R)/a_{11}$, while $\bar{P} = 0$ in paraelectric phase. Depolarization field and surface influence lead to the renormalization of coefficient a_1 in Eq. (7) as[25]

$$a_R(T,R) \approx \alpha_T \left[T - T_c \left(1 - \frac{R_{\mathrm{cr}}^0}{R} \right) \right], \tag{8}$$

where $R_{\mathrm{cr}}^0 = 3\xi/\alpha_T T_c(\lambda + \sqrt{\xi\varepsilon_0})$ is a critical radius of size-induced paraelectric phase appearance at zero temperature and $R < R_{\mathrm{cr}}$. It exists at $\lambda > -\sqrt{\xi\varepsilon_0}$, and thus we consider the case of the positive extrapolation length hereinafter. At a given temperature T the sphere critical radius $R_{\mathrm{cr}}(T) \approx R_{\mathrm{cr}}^0/1 - T/T_c$ exists at $T < T_c$ and should be found from the condition $a_R(T, R_{\mathrm{cr}}) = 0$. Both measured and calculated values of R_{cr} typically depend on temperature T and varied within the range 2–50 nm.[26–28] At radii $R \gg R_{\mathrm{cr}}(T)$ the particles' ferroelectric properties are close to the bulk material.

In plane, perpendicular to the polar axis ($k_3 = 0$), the expression (7) can be simplified to a Lorentzian form $\tilde{\chi}(\mathbf{k}) \sim [R_{cx}^2(k_1^2 + k_2^2) + 1]^{-1}$, where the correlation radii for the fluctuations across polar axis are introduced as

$$R_{cx}(T,R) = \begin{cases} \sqrt{\dfrac{\eta}{a_R(T,R)}}, & a_R(T,R) > 0 \\ \sqrt{\dfrac{-\eta}{2a_R(T,R)}}, & a_R(T,R) < 0. \end{cases} \tag{9}$$

Since usually gradient coefficients $\xi \sim \eta$, while for ferroelectrics $a_1\varepsilon_0 \ll 1$, the longitudinal correlation radius R_{cz} is almost constant and much smaller than R_{cx}. This means that the depolarization field suppresses longitudinal fluctuations.[24]

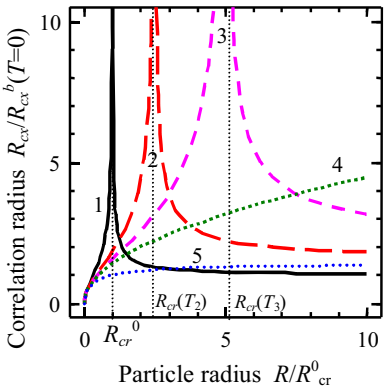

FIG. 2. (Color online) Transverse correlation radius $R_{cx}/R_{cx}^b(T=0)$ dependence on particle radius R/R_{cr}^0 for different temperatures below ($T < T_c$), equal ($T = T_c$), and above ($T > T_c$) the bulk transition temperature T_c; $T/T_c = 0$, 0.6, 0.8, 1, and 2 (curves 1–5). Bulk correlation radius $R_{cx}^b = \sqrt{-\eta/2a_1(T)}$ is defined in ferroelectric phase ($T < T_c$).

Transverse correlation radius R_{cx} dependence via the particle radius calculated on the basis of Eq. (9) is shown in Fig. 2. At temperatures $T < T_c$ transverse correlation radius R_{cx} diverges at critical radius $R_{cr}(T)$ as anticipated from Eq. (9) (see curves 1–3). The divergence corresponds to the size-induced ferroelectric-paraelectric phase transition. At temperatures $T > T_c$ transverse correlation radius monotonically increases with the particle radius because of $a_R^{-1}(T,R)$ increase (see curves 4 and 5).

III. POTENTIAL BARRIER FOR POLARIZATION REORIENTATION IN FERROELECTRIC NANOPARTICLES

In the vicinity of the phase-transition polarization reorientation is caused by fluctuations. So, let us study the question how high can the potential barrier of polarization reorientation in spherical ferroelectric nanoparticles under the absence of external field be.

A. Barrier for perovskite and uniaxial ferroelectric nanoparticles

For uniaxial ferroelectrics the barrier between the states $\pm P_0$ can be estimated on the basis of the free energy

$$F(\bar{\mathbf{P}}) = V\left(\frac{a_R(T,R)}{2}\bar{P}^2 + \frac{a_{11}}{4}\bar{P}^4 - \bar{P}E_0 \right). \tag{10}$$

In Eq. (10) the integration over the spherical particle volume $V = 4\pi R^3/3$ was performed. At zero external electric field ($E_0 = 0$) the barrier $\Delta F = V a_R^2(T,R)/4a_{11}$.

For perovskite ferroelectrics the orientation barrier can be estimated on the basis of the free energy

$$F(\bar{\mathbf{P}}) = V\left(\frac{a_R(T,R)}{2}(\bar{P}_1^2+\bar{P}_2^2+\bar{P}_3^2)+\frac{a_{12}}{2}(\bar{P}_1^2\bar{P}_2^2+\bar{P}_3^2\bar{P}_2^2 + \bar{P}_3^2\bar{P}_1^2)+\frac{a_{11}(T,R)}{4}(\bar{P}_1^4+\bar{P}_2^4+\bar{P}_3^4)-\bar{P}_1E_{01}-\bar{P}_2E_{02} - \bar{P}_3E_{03}\right). \quad (11)$$

Free energy (11) is stable only for $a_{11}>0$ and $a_{11}+2a_{12}>0$, otherwise one should consider higher order terms in Eq. (11). At zero external electric field, $E_0=0$, free energy (11) can describe paraelectric (PE) phase with $\bar{P}_i=0$ (thermodynamically stable at $a_R>0$); rhombohedral ferroelectric (rFE) phase with $\bar{P}_1^2=\bar{P}_2^2=\bar{P}_3^2=-a_R/(a_{11}+2a_{12})$ (stable at $a_R<0$ and $a_{11}>a_{12}$); tetragonal ferroelectric (tFE) phase with $\bar{P}_i^2=-a_R/a_{11}$, $\bar{P}_j^2=\bar{P}_k^2=0$, and $i\neq j\neq k$ (stable at $a_R<0$ and $a_{11}<a_{12}$). The saddle points $\bar{P}_i^2=\bar{P}_j^2=-a_R/(a_{11}+a_{12})$ and $\bar{P}_k^2=0$, bordering the minima exist in tFE. One can find the potential barrier between different polarization orientations in stable phases as a difference between the free-energy values corresponding to minimum and saddle point. Thus, using Eqs. (10) and (11), we have found the reorientation barrier in the form

$$\Delta F(T,R) = \gamma(T,R)\cdot k_BT,$$

$$\gamma(T,R) = V\frac{a_R^2(R,T)}{4k_BT\,a_{11}}\begin{cases}\dfrac{a_{12}-a_{11}}{a_{12}+a_{11}}, & 2a_{11}<a_{12}, \quad \text{perovskite FE}\\ \dfrac{a_{11}}{a_{11}+2a_{12}}\left(\dfrac{a_{11}-a_{12}}{a_{12}+a_{11}}\right), & 2a_{11}>a_{12}, \quad \text{perovskite FE}\\ 1, \quad \text{uniaxial FE.}\end{cases} \quad (12)$$

Here the dimensionless barrier height γ is introduced.

Note that Eq. (11) transforms into Eq. (10) at $a_{11}=a_{12}$ with accuracy of multiplayer 3. In this "isotropic" case the barrier and the circle of minima looks like "sombrero."

Examples of the phase diagrams in coordinate temperature sizes are shown in Fig. 3 for perovskite [Figs. 3(a) and 3(b)] and uniaxial [Figs. 3(c) and 3(d)] ferroelectric nanoparticles. Solid curves correspond to the transition between paraelectric and ferroelectric phases, i.e., it is the dependence $T_{cr}(R)$ and so $\Delta F(T_{cr},R)=0$. Dashed curves represent the situation when the reorientation barrier is equal to the energy of thermal fluctuations $\Delta F=k_BT$; dotted curves correspond to barriers $\Delta F=2k_BT$ [Figs. 3(a) and 3(b)] and $50k_BT$ [Figs. 3(c) and 3(d)]. Filled area between corresponding solid and dashed curves indicates the regions with potential barrier ΔF lower than the thermal activation energy.

Freezing temperature $T_f(R_0)$ at a given particle radius R_0 can be estimated as an intersection of the vertical line $R=R_0$ with corresponding dashed (or dotted) curves as shown in Fig. 3(a). So at a given particle radius R_0 *free reorientation* of polarization is expected in the temperature range $T_f(R_0)<T<T_{cr}(R_0)$. Similarly, at fixed temperature T_0 the "freezing" nanoparticle radius $R_f(T_0)$ can be estimated an intersection of the horizontal line $T=T_0$ with corresponding dashed (or dotted) curves shown in Fig. 3(a). Surely the range determination is somehow voluntary, since the value of $T_f(R)$ or $R_f(T)$ depends on numerical factor γ before k_BT that in turn depends on the system characteristics.

Dashed curves represent the situation when the reorientation barrier is equal to the energy of thermal fluctuations, $\Delta F=k_BT$; dotted curves correspond to barriers $\Delta F=2k_BT$ [Figs. 3(a) and 3(b)] and $50k_BT$ [Figs. 3(c) and 3(d)]. Groups of curves 1, 2, and 3 correspond to critical radius at zero temperature $R_{cr}^0=0.4$, 1, and 3 nm. Coefficients for $BiFeO_3$ were taken from Ref. 29, namely, $a_1=9.8(T-1103)\times10^5$ $(C^{-2}m^2N)$ with temperature in kelvin, $a_{11}=13\times10^8$ $(C^{-4}m^6N)$, and $a_{12}=2\times10^8$ $(C^{-4}m^6N)$. Coefficients for $PbZr_xTi_{1-x}O_3$ can be found in Ref. 30. Free-energy expan-

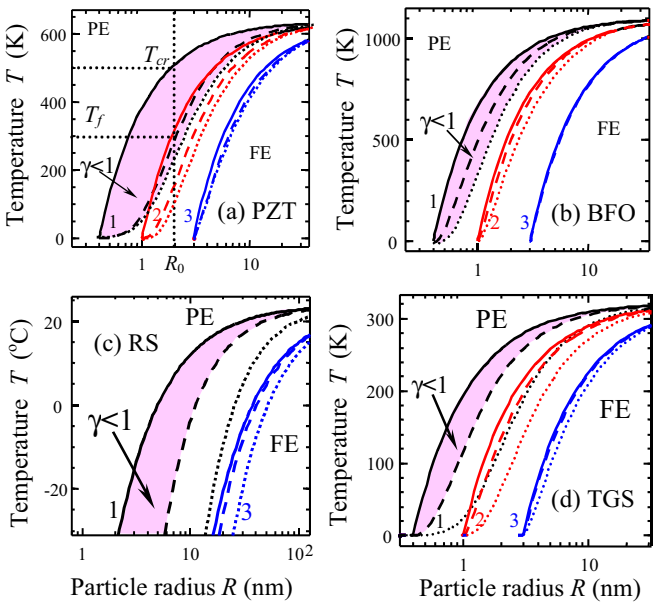

FIG. 3. (Color online) Phase diagram in coordinate temperature size for four different sets of material parameters corresponding to $PbZr_{0.6}Ti_{0.4}O_3$ (PZT), $BiFeO_3$ (BFO), Rochelle salt (RS), and triglycine sulfate (TGS) (panels a, b, c, and d, respectively). Solid curves are related to the transition between paraelectric and ferroelectric (FE) phases, i.e., it is $T_{cr}(R)$, where $\Delta F=0$.

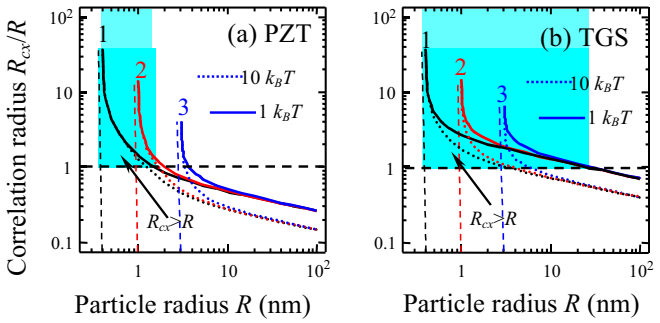

FIG. 4. (Color online) (a) and (b) The dependence of ratio $R_{cx}(T,R)/R$ on particle radius R for orientation barrier k_BT (solid curves) and $10k_BT$ (dotted curves) and different values of critical radius R^0_{cr}=0.4, 1, and 3 nm (curves 1–3). Vertical lines indicate the FE-PE phase transition appearing at critical radius R^0_{cr}; $R^b_{cx}(T=0)$ =1 nm (other material parameters are the same as in Fig. 3). Filled area reflects the region of superparaelectric phase existence.

sion coefficients for RS and TGS were calculated from data given in Ref. 31.

So at fixed radius R, superparaelectric (SPE) phase may appear only in the temperature range $T_f(R)<T<T_{cr}(R)$. At fixed temperature (e.g., at room) SPE may appear only at nanoparticle radii $R_{cr}(T)<R<R_f(T)$. However, as was stated in Sec. I, the condition of all ions inside the particle alignment is necessary for SPE appearance [see Fig. 1(b)]. As we have discussed in Sec. I to superparamagnetic nanoparticles, the alignment due to the correlation effects is possible when the particle radius R is less than the correlation radius R_c. On the other hand the particle radius must be higher than the critical radius R_{cr} of size-driven ferroelectric-paraelectric phase transition. Therefore we have to find out the region of radii where the conditions can be fulfilled.

B. Correlation effect in ferroelectric nanoparticles

The dependence of ratio $R_{cx}(T,R)/R$ on particle radius R for the temperatures T corresponding to orientation barrier $\Delta F(T,R)=k_BT$ (solid curves) and $\Delta F(T,R)=10k_BT$ (dotted curves) are shown in Figs. 4(a) and 4(b) for PZT and TGS, respectively. In the range $\infty>R_{cx}(T,R)/R>1$ the alignment of elementary dipoles appears due to the correlation effects as well as adopted here long-wave approximation is valid and self-consistent. So, the filled area between solid curves $[\Delta F(T,R)=k_BT]$, dashed vertical lines of size-induced FE-PE phase transition ($R=R^0_{cr}$ and $\Delta F=0$), and horizontal line ($R_{cx}=R$) indicates the region of particle radii corresponding to the possible superparaelectric phase appearance.

It is seen from Fig. 4 that the region of SPE phase can be large enough, its width being essentially dependent on existence of low barrier, and the region is broader for TGS than for PZT.

In agreement with Eq. (12), energetic barrier height $\Delta F(R)\sim R^3\alpha_T^2/a_{11}\sim V R_{cx}^{-2}\bar{P}_0^2$. So to obtain low barriers in the wider vicinity of PE-FE size-induced phase transition, high R_{cx}, low $\bar{P}_0^2$ values, and small enough particle radii are necessary. The favorable conditions for small ΔF and high R_{cx} values are small Curie-Weiss constants and high coefficients a_{11}.

To summarize, the condition $0<\Delta F(T,R)\leq k_BT$ determines the superparaelectric phase appearance in ferroelectric nanoparticles of radius $R_{cr}(T)<R<R_f(T)<R_c(T)$ at given temperature T or alternatively at temperatures $T_f(R)<T<T_{cr}(R)$ at given radius R. In the region of relatively low potential barrier of polarization reorientation under *external electric field* could partially or fully align the nanoparticle dipoles as considered below.

We have to underline that, namely, aforementioned temperature-size region corresponds to the true SPE phase. In this region polarization of free orientable dipoles has to be independent on the regime of external electric-field application (field cooling, zero-field cooling, etc.) so here the behavior of SPE is ergodic. In what follows we will consider the influence of external electric field on polarization for two cases, namely, for k_BT larger and smaller than the barrier for dipole reorientation. In the latter case the hysteresis loop can appear at $T<T_f(R)$ that is known to be characteristic feature of ferroelectric phase. One can also expect the transformation of behavior into nonergodic one with dependence of polarization response on the regime of field application like it was observed for superparamagnetic phase.[32] On the other hand the behavior in the region $T<T_b$ is considered as "blocked superparamagnetism" in Ref. 4. In any case it is obvious that the region $T<T_f$ has to be included into consideration of superparaelectrics.

IV. POLARIZATION RESPONSE TO EXTERNAL FIELD

At a given temperature T and nanoparticle radius R, polarization orientation with respect to external field $\mathbf{E}_0=\{0,0,E_0\}$ can be written as $\mathbf{P}=\{P\sin\theta\cos\varphi, P\sin\theta\sin\varphi, P\cos\theta\}$. After elementary transformations the free energies (10) and (11) acquire the form

$$F(\bar{P},\theta,\varphi)=V\begin{cases}\left(\begin{array}{l}\dfrac{a_R(T,R)}{2}\bar{P}^2+\dfrac{a_{11}}{4}\bar{P}^4-E_0\bar{P}\cos\theta+\\ \dfrac{(a_{12}-a_{11})}{2}\bar{P}^4(\sin^4\theta\sin^2\varphi\cos^2\varphi+\sin^2\theta\cos^2\theta)+\end{array}\right) & \text{perovskite FE}\\ \left(\dfrac{a_R(T,R)}{2}\bar{P}^2+\dfrac{a_{11}}{4}\bar{P}^4-E_0\bar{P}\cos\theta\right), & \text{uniaxial FE}\end{cases}. \quad (13)$$

Here $\{\theta,\varphi\}$ are the spherical angles. Similarly to the consideration of superparamagnetics proposed by Binder and Young,[3] in order to obtain *equilibrium* polarization vector $\langle \mathbf{P}(E_0)\rangle=\{P_1,P_2,P_3\}$, polarization components $P_i(E_0,\theta,\varphi)$ should be averaged over the spherical angles $\{\theta,\varphi\}$ and polarization absolute value $\bar{P}$ distribution

$$\langle \bar{P}_i(E_0)\rangle = \int_0^\infty d\bar{P}\,\mu(\bar{P})\exp\left[-\frac{F_0(\bar{P})}{k_BT}\right] \times \frac{\int_0^{2\pi}d\varphi\int_0^{\pi}d\theta\,\sin\theta\exp[-F_a(\bar{P},\theta,\varphi)/k_BT]\,\bar{P}_i(E_0,\theta,\varphi)}{\int_0^{2\pi}d\varphi\int_0^{\pi}d\theta\,\sin\theta\exp[-F_a(\bar{P},\theta,\varphi)/k_BT]}. \tag{14}$$

Here $\mu(\bar{P})$ is the distribution function of $\bar{P}$, originated from the dispersion of nanoparticle sizes R, schematically shown in Fig. 1(a).

$F_0(\bar{P})=V(R)(\frac{a_R(R,T)}{2}\bar{P}^2+\frac{a_{11}}{4}\bar{P}^4)$ is the isotropic part (i.e., angles independent) of the free energy (13) that coincides with Eq. (10) at $E_0=0$; $F_a(\bar{P},\theta,\varphi)$ is the angle-dependent part. Note that due to the conservation of magnetization vector absolute value, the isotropic part F_0 does not play any important role in superparamagnetics consideration (paraprocess is typically small).[1,2] However, in ferroelectrics polarization absolute value strongly depends on the boundary conditions and applied electric field so F_0 is essential.

The averaging over the spherical angles in Eq. (14) leads to the dependences $\langle P_1(E_0)\rangle=\langle P_2(E_0)\rangle=0$. Note that *equilibrium* (or *absolutely stable*) remnant polarization is always absent, i.e., $\langle P_3(E_0=0)\rangle=0$. Actually, the free energy (13) is the even function of $\cos\theta$ at $E_0=0$, while $P_3=\bar{P}\cos\theta$ is an odd function of $\cos\theta$, and so at zero applied field only the trivial solution $\langle P_3(E_0=0)\rangle=\bar{P}\langle\cos\theta\rangle\equiv 0$ exists. The mathematical result reflects the conventional statement that *equilibrium* polarization of perfect ferroelectrics can be reversed by infinitely small field applied long enough.[31,33] In other words, hysteresis phenomenon appearance at $T\ll T_f(R)$ [or nanoparticle radiuses $R\gg R_f(T)$] has to correspond to the *metastable (nonergodic) state*. In order to include bistable states (e.g., hysteresis) averaged values $\langle P_i\rangle$ should be substituted either into Eq. (14) or in the free energy (13) *self-consistently*.[15]

In what follows we will consider separately the nanoparticles of the uniaxial and perovskite ferroelectrics allowing for the different forms of their free energy and barriers.

A. Uniaxial ferroelectrics

For uniaxial ferroelectrics, analytical integration on the spherical angles $\{\theta,\varphi\}$ can be performed in Eq. (14). This leads to the expression

$$\langle \bar{P}_3(E_0)\rangle = \int_0^\infty d\bar{P}\,\mu(\bar{P})\bar{P}\exp\left(-\frac{F_0(\bar{P})}{k_BT}\right)L\left(\frac{VE_0\bar{P}}{k_BT}\right),$$

$$L(x)=\frac{1}{\tan h(x)}-\frac{1}{x}. \tag{15}$$

Function $L(x)$ is exactly Langevin function. Independent on electric field and related to the barrier exponential term with isotropic part of the free energy F_0 is the additional factor in comparison with superparamagnetics.

It is clear from Eq. (15) that the Langevin law can be obtained for infinitely sharp Dirac-delta distribution function $\mu(P)=\delta(P-\bar{P})$ (i.e., all particles have equal radius) and low energetic barriers $|F_0(\bar{P})|\ll k_BT$ so $\exp(-F_0/k_BT)\approx 1$ [i.e., particle radius is much smaller than the freezing radius $R\ll R_f(T)$], namely, for the case

$$\langle \bar{P}_3(E_0)\rangle \approx \bar{P}\tan\ h^{-1}\left(\frac{VE_0\bar{P}}{k_BT}\right)-\frac{k_BT}{VE_0}. \tag{16}$$

Surely, in a given nanocomposite sample nanoparticle sizes are distributed. For this case the averaging in Eq. (15) with finite-width distribution function $\mu(P)$ should be performed. Obtained results essentially depend on distribution function parameters, however in any case one can obtain Langevin-like behavior for sharp enough distribution function $\mu(P)$ and low energetic barriers. Langevin-like behavior in superparamagnetic was obtained in Ref. 4; the phenomenon was called isotropic supermagnetism.

At fixed temperature (e.g., at room) and nanoparticle radius essentially higher than the "freezing radius" $R\gg R_f(T)$, orientation barrier is much higher than the thermal fluctuations k_BT. So, lets divide the integration on the particle radius in Eq. (15) into two regions $0<R<R_f(T)$ and $R>R_f(T)$. Region $0<R<R_f(T)$ (and so $R<R_c$ since $R_f<R_c$) corresponds to the behavior without hysteresis, since here the barrier $|F_0(\bar{P})|<k_BT$ and so $\exp\sim 1$. Region $R\gg R_f(T)$ (and so $R\gg R_c$), where $|F_0(\bar{P})|\gg k_BT$, has to be ferroelectric phase that could be considered self-consistently, namely, with the substitution $P^4\sim P^2\langle P_3\rangle^2$ in the free energy F_0. Using these ideas and Laplace method of integration, we obtained approximate analytical expressions

$$\langle \bar{P}_3(E_0)\rangle \approx \int_0^{R_f(T)} dR\,\tilde{\mu}(R)\bar{P}(R)L\left(\frac{VE_0\bar{P}(R)}{k_BT}\right) + \int_{R_f(T)}^\infty \frac{dR\,\tilde{\mu}(R)\,E_0}{a_R(R,T)+a_{11}\langle \bar{P}_3(E_0)\rangle^2}. \tag{17}$$

Here $\tilde{\mu}(R)$ is the normalized distribution function of nanoparticle radii R, related with $\mu(\bar{P})$ in conventional way (see, e.g., Ref. 34), and $\bar{P}$ satisfies the equation $a_R(T,R)\bar{P}+a_{11}\bar{P}^3=E_0$. Note, that $R_{cr}(T)<R_f(T)<R_c(T)$ as stated in Sec. III. Thus in the first integral $R<R_c$, while in the second integral both regions $R<R_c$ and $R>R_c$ are included. Note, that we did not consider the critical region $R\approx R_{cr}(T)$, where the critical phenomena can be important.

Dependence of mean polarization $\langle P_3\rangle$ on the applied electric field is shown in Fig. 5(a) for uniaxial RS material parameters, Dirac-delta distribution $\tilde{\mu}(R)=\delta(R-R_0)$ of particle sizes, fixed freezing radius $R_f(T)$ at room temperature

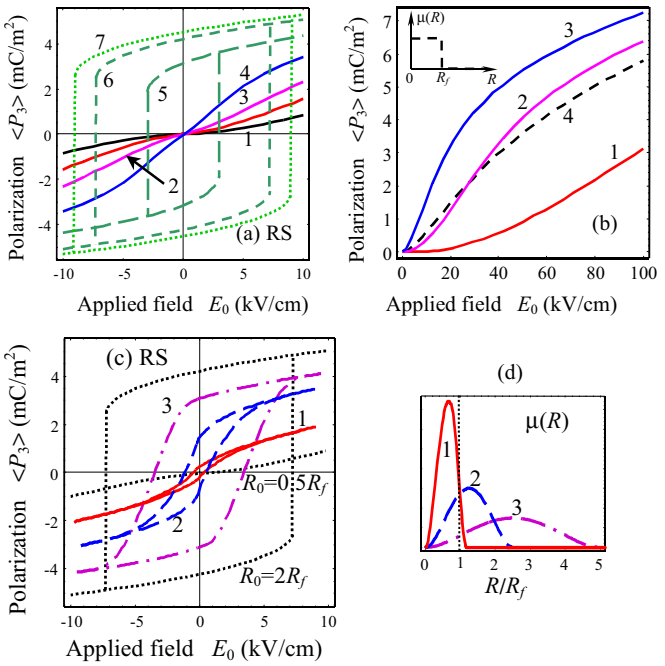

FIG. 5. (Color online) (a) Dependence of Rochelle salt polarization $\langle P_3(E_0)\rangle$ on the applied electric field E_0 calculated from Eq. (17) for Dirac-delta distribution $\tilde{\mu}(R)=\delta(R-R_0)$ and different values R_0=6, 7, 8, 9, 11, 20, and 30 nm (Figs. 1–7 near curves). The freezing radius R_f=10 nm at temperature T=273 K, R_{cr}^0=0.5 nm. (b) Dependence $\langle P_3(E_0)\rangle$: solid curves 1–3 are Langevin law (16) for different nanoparticle radii R=3, 5, and 7 nm; dashed curve 4 corresponds to Eq. (17) with rectangular distribution function, $\tilde{\mu}(R)=1/R_f$ at $0<R<R_f$, shown in the inset. (c) Dependence $\langle P_3(E_0)\rangle$ calculated from Eq. (17) for well-localized distribution functions $\tilde{\mu}(R)$ (curves 1–3) shown in inset (d). Dotted curves correspond to Dirac-delta distribution $\tilde{\mu}(R)=\delta(R-R_0)$ for $R_0=0.5R_f$ and $R_0=2R_f$ (labels near the curves). Other material parameters are the same as in Fig. 3(c).

T=0 °C, and different nanoparticle average radius R_0. Curves 1–4 for $R_0<R_f$ correspond to the Langevin law, while curves 5–7 for $R_0>R_f$ indicate the hysteresis loop appearance.

Solid curves in Fig. 5(b) are Langevin law $\langle \bar{P}_3(E_0)\rangle$ for different nanoparticle radii R; dashed curve corresponds to the rectangular distribution function $\tilde{\mu}(R)=1/R_f$ at $0<R<R_f$ shown in the inset.

Dependence $\langle P_3(E_0)\rangle$ calculated from Eq. (17) for bell-shaped distribution functions $\tilde{\mu}(R)$ is shown in Fig. 5(c) (curves 1–3). Dotted curves correspond to Dirac-delta distribution $\tilde{\mu}(R)=\delta(R-R_0)$ for small $R_0<R_f$ and high $R_0>R_f$.

It follows from Fig. 5 that for Langevin-like behavior besides small enough nanoparticle radii and barrier (as it was discussed earlier) the narrow distribution function of the particle radii and polarization is necessary, the particular form of distribution function being not especially important. It is obvious also that hysteresis loop originates from contribution of either large enough average particles radii [see Fig. 5(a)] or broad distribution function [see Figs. 5(c) and 5(d)]. The important role of large particles in appearance of hysteresis loop is similar to what obtained in superparamagnetism earlier.[4] Allowing for this behavior at $T<T_b$ to be named as blocked superparamagnetism, it seems reasonable to name the region $T<T_f$ with hysteresis loop as frozen superparaelectricity.

B. Perovskite ferroelectrics

For perovskite ferroelectrics with $a_{11}\neq a_{12}$, the averaging on the angle φ in Eq. (14) leads to the expression

$$\langle \bar{P}_3(E_0)\rangle = \int_0^\infty d\bar{P}\,\mu(\bar{P})\exp\left(-\frac{F_0(\bar{P})}{k_BT}\right) \times \bar{P}\frac{\int_0^\pi d\theta \sin\theta\cos\theta\, K(\bar{P},\theta)}{\int_0^\pi d\theta \sin\theta\, K(\bar{P},\theta)},$$

$$K(\bar{P},\theta)=2\pi\exp\left(-\frac{\Delta F_a(\bar{P},\theta)}{k_BT}\right)I_0\left(V\frac{(a_{12}-a_{11})\bar{P}^4}{16k_BT}\sin^4\theta\right),$$

$$\Delta F_a(\bar{P},\theta)=V\left(\frac{a_{12}-a_{11}}{2}\bar{P}^4\sin^2\theta\cos^2\theta + \frac{(a_{12}-a_{11})\bar{P}^4}{16}\sin^4\theta - E_0\bar{P}\cos\theta\right). \quad (18)$$

I_0 is the modified Bessel function of zero order.

Similarly to the case of uniaxial ferroelectrics, let us divide the averaging on the particle radius in Eq. (18) into two regions $0<R<R_f(T)$ and $R>R_f(T)$. In the region $0<R<R_f(T)$, the barrier is $|F_0(\bar{P})|<k_BT$, and so $\exp\sim 1$. The ferroelectric region $R\gg R_f(T)$, where $|F_0(\bar{P})|\gg k_BT$, was considered self-consistently. Similarly to Eq. (17), we obtained approximate analytical expressions

$$\langle \bar{P}_3(E_0)\rangle \approx \int_0^{R_f(T)} dR\,\tilde{\mu}(R)\bar{P}\frac{\int_0^\pi d\theta \sin\theta\cos\theta\, K(\bar{P},\theta)}{\int_0^\pi d\theta \sin\theta\, K(\bar{P},\theta)} + \int_{R_f(T)}^\infty \frac{dR\,\tilde{\mu}(R)\,E_0}{a_R(R,T)+a_{11}\langle \bar{P}_3(E_0)\rangle^2}. \quad (19)$$

Here $\tilde{\mu}(R)$ is the normalized distribution function of nanoparticle radii R and $\bar{P}$ satisfies the equation $a_R(T,R)\bar{P}+a_{11}\bar{P}^3=E_0$.

Dependence of mean polarization $\langle P_3\rangle$ on the applied electric field is shown in Fig. 6(a) for perovskite PZT material parameters, Dirac-delta distribution $\tilde{\mu}(R)=\delta(R-R_0)$, fixed temperature $T<T_c$, freezing radius $R_f(T)$, and different nanoparticle radius R_0. Curves 1–4 for $R_0<R_f$ correspond to the Langevin-like law, while the curves 5–7 for $R_0>R_f$ indicate the hysteresis loop appearance. Solid curves in Fig. 6(b) are Langevin-like law $\langle P_3(E_0)\rangle$ for different nanoparticle radius R; dashed curve corresponds to the rectangular

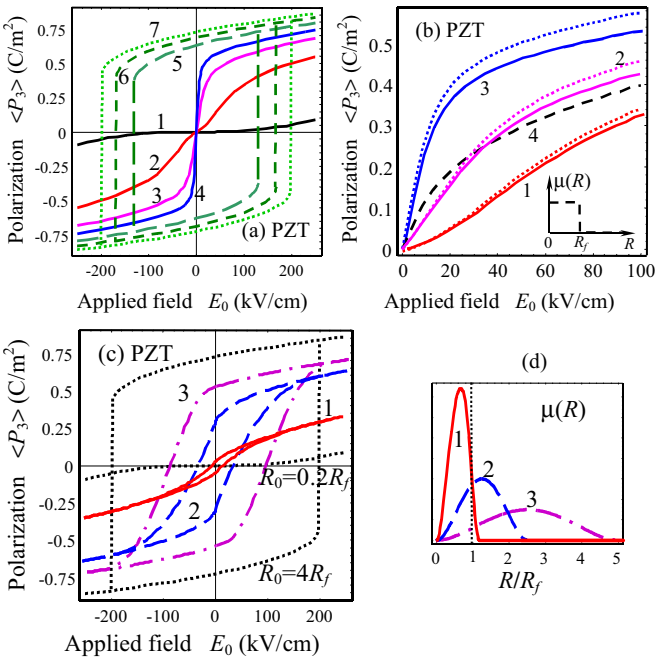

FIG. 6. (Color online) (a) Dependence of $PbZr_{0.6}Ti_{0.4}O_3$ (PZT) polarization $\langle P_3(E_0)\rangle$ on the applied electric field E_0 calculated from Eq. (19) for Dirac-delta distribution $\tilde{\mu}(R)=\delta(R-R_0)$ and different values R_0=0.5, 1, 1.5, 2, 3, 5, and 10 nm (Figs. 1–7 near curves). The freezing radius R_f=2.5 nm at room temperature T=293 K, R_{cr}^0=0.5 nm. (b) Dependence $\langle P_3(E_0)\rangle$: curves 1–3 are Langevin law (dotted curves) and Langevin-like law (solid curves) calculated from Eq. (19) for different nanoparticle radius R=1, 1.2, and 1.6 nm; dashed curve 4 corresponds to the rectangular distribution function, $\tilde{\mu}(R)=1/R_f$ at $0<R<R_f$, shown in the inset. (c) Dependence $\langle P_3(E_0)\rangle$ calculated from Eq. (19) for well-localized distribution functions $\tilde{\mu}(R)$ (curves 1–3) shown in inset (d). Dotted curves correspond to Dirac-delta distribution $\tilde{\mu}(R)=\delta(R-R_0)$ for $R_0=0.2R_f$ and $R_0=4R_f$ (labels near the curves). Other material parameters are the same as in Fig. 3(a).

distribution function $\tilde{\mu}(R)$ shown in the inset. Dependence $\langle P_3(E_0)\rangle$ calculated from Eq. (19) for well-localized distribution functions $\tilde{\mu}(R)$ is shown in Fig. 5(c) (curves 1–3).

It follows from Fig. 6 that qualitatively the curves look like those depicted in Fig. 5 for uniaxial case. Namely, the narrower the distribution function of sizes the better is the condition of Langevin type behavior observation.

One can see from Fig. 6(b) that pure Langevin curves are higher than solid curves for different radii. Similarly to superparamagnetics case,[4] this behavior could be named as *anisotropic superparaelectricity* because of barrier anisotropy $(a_{11}-a_{12})$ contribution in perovskites [see Eq. (18)].

To summarize the Sec. IV, Langevin-like law for polarization dependence on external field was predicted in the temperature range $T_{cr}(R)>T>T_f(R)$ at fixed radius $R<R_f$ [or in the range $R_{cr}(T)<R<R_f(T)$ at fixed temperature T]. Bistable remnant polarization appeared at temperatures $T<T_f(R)$ [or at radii $R\gg R_f(T)$]. For nanoparticle radius less than critical both hysteresis and its precursor, Langevin-like behavior, are smeared.

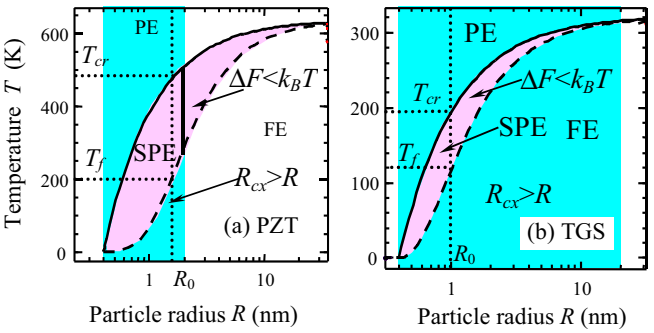

FIG. 7. (Color online) SPE phase region for (a) PZT and (b) TGS. Material parameters are listed in Fig. 3.

V. SUPERPARAELECTRICITY AND THE CONDITIONS OF ITS EXPERIMENTAL OBSERVATION

The overlap of filled regions from Fig. 3 $[T_f(R)<T<T_{cr}(R)]$ and corresponding radii range $(R_{cr}<R<R_c)$ from Fig. 4 gives SPE phase region as shown in Fig. 7 for PZT [Fig. 7(a)] and TGS [Fig. 7(b)].

At low temperatures $T\to 0$ [and so $R_{cr}(T)\to R_{cr}^0$], approximate expression for the freezing temperature T_f could be obtained from the condition $\gamma(T_f,R\to R_{cr}^0)=1$ [see Eq. (12)], namely, we obtained the parabolic law

$$T_f(R\to R_{cr}^0)\approx \frac{\pi R_{cr}^0 C_0}{3k_B a_{11}}[\alpha_T T_c(R-R_{cr}^0)]^2. \qquad (20)$$

Constant C_0 depends on coefficients a_{11} and a_{12} only, as given by Eq. (12) for γ.

To summarize, let us formulate the conditions of superparaelectric phase appearance in the ensemble of noninteracting ferroelectric particles of spherical shape and their property peculiarities, which can be considered as characteristic features of SPE phase.

(1) The superparaelectric phase can appear in ferroelectric nanoparticles of average radius $R_{cr}<R<R_c$ at temperatures $T_f(R)<T<T_{cr}(R)$. In this region:

(a) All nanoparticle dipole moments are aligned due to the correlation effects.

(b) Potential barrier of polarization reorientation is smaller than the thermal activation energy $\sim k_BT$.

(c) Langevin-like law for polarization dependence on external field is valid at temperatures higher than the freezing temperature $T_f(R)$, but lower than the temperature $T_{cr}(R)$ of size-driven ferroelectric-paraelectric phase transition.

(d) Hysteresis loop and remnant polarization (frozen SPE) appear at temperatures $T<T_f(R)$.

(e) The observation time of the experiment t should be larger than characteristic time τ of particle reorientation in external field. The time τ is given by the Arrhenius law, $\tau=\tau_0\exp(\Delta F/k_BT)$, where the barrier height ΔF is proportional to the particle volume V in accordance with Eq. (12) and the phonon time $\tau_0\sim 10^{-12}$ s, so that the characteristic time τ has to be small enough for the small particles and condition $t>\tau$ has to be fulfilled.

(2) The favorable conditions for the superparaelectricity observation in small ferroelectric nanoparticles at room tem-

peratures are small Curie-Weiss constant, high nonlinear coefficients a_{11}, and narrow distribution function of particle radii. The ensemble of noninteracting ferroelectric nanoparticles could be realized in nanoporous nonferroelectric matrix with the porous filled at least partly by some ferroelectric material. Another type of composite material with cylindrical geometry of nanoporous in the nonferroelectric matrix filled with ferroelectric nanorods cannot be excluded also. However some differences in polar behaviors for this geometry in comparison with spherical case can be expected.

The theoretical forecast is waiting for experimental revealing.

*Corresponding author. Permanent address: V. Lashkarev Institute of Semiconductor Physics, NAS of Ukraine, 41, pr. Nauki, 03028 Kiev, Ukraine; morozo@i.com.ua

[1] V. K. Wadhawan, *Introduction to Ferroic Materials* (Gordon and Breach, New York, 2000).
[2] E. Roduner, *Nanoscopic Materials: Size-Dependent Phenomena* (RSC, Cambridge, 2006).
[3] K. Binder and A. P. Young, Rev. Mod. Phys. **58**, 801 (1986).
[4] F. Wiekhorst, E. Shevchenko, H. Weller, and J. Kotzler, Phys. Rev. B **67**, 224416 (2003).
[5] Y. Kumzerov and S. Vakhrushev, in *Encyclopedia of Nanoscience and Nanotechnology*, edited by H. S. Halwa (American Scientific Publishers, Stevenson Ranch, 2003), Vol. 10, pp. 1–39.
[6] F. D. Morrison, Y. Luo, I. Szafraniak, V. Nagarajan, R. B. Wehrspohn, M. Steinhart, J. H. Wendroff, N. D. Zakharov, E. D. Mishina, K. A. Vorotilov, A. S. Sigov, S. Nakabayashi, M. Alexe, R. Ramesh, and J. F. Scot, Rev. Adv. Mater. Sci. **4**, 114 (2003).
[7] D. Yadlovker and S. Berger, Phys. Rev. B **71**, 184112 (2005).
[8] L. E. Cross, Ferroelectrics **76**, 241 (1987).
[9] Sh. Li, J. A. Eastman, R. E. Newnham, and L. E. Cross, Phys. Rev. B **55**, 12067 (1997).
[10] A. E. Glazounov, A. J. Bell, and A. K. Tagantsev, J. Phys.: Condens. Matter **7**, 4145 (1995).
[11] H. Kohlstedt, Y. Mustafa, A. Gerber, A. Petraru, M. Fitsilis, R. Meyer, U. Bottger, and R. Waser, Microelectron. Eng. **80**, 296 (2005).
[12] A. Roelofs, T. Schneller, K. Szot, and R. Waser, Appl. Phys. Lett. **81**, 5231 (2002).
[13] R. Tiruvalam, A. Kundu, A. Soukhojak, S. Jesse, and S. V. Kalinin, Appl. Phys. Lett. **89**, 112901 (2006).
[14] M. E. Lines and A. M. Glass, *Principles and Application of Ferroelectrics and Related Materials* (Clarendon, Oxford, 1977).
[15] V. G. Vaks, *Introduction to the Microscopic Theory of Ferroelectricity* (Nauka, Moscow, 1973).
[16] R. Blinc and B. Zeks, *Soft Mode in Ferroelectrics and Antiferroelectrics* (North-Holland, Amsterdam, 1974).
[17] M. D. Glinchuk, E. A. Eliseev, and A. N. Morozovska, arXiv:0806.2127 (unpublished).
[18] R. Kretschmer and K. Binder, Phys. Rev. B **20**, 1065 (1979).
[19] I. I. Naumov, L. Bellaiche, and H. Fu, Nature (London) **432**, 737 (2004).
[20] I. Ponomareva, I. I. Naumov, I. Kornev, H. Fu, and L. Bellaiche, Phys. Rev. B **72**, 140102(R) (2005).
[21] S. Prosandeev, I. Ponomareva, I. Naumov, I. Kornev, and L. Bellaiche, J. Phys.: Condens. Matter **20**, 193201 (2008).
[22] J. Slutsker, A. Artemev, and A. Roytburd, Phys. Rev. Lett. **100**, 087602 (2008).
[23] C.-L. Jia, V. Nagarajan, J.-Q. He, L. Houben, T. Zhao, R. Ramesh, K. Urban, and R. Waser, Nature Mater. **6**, 64 (2007).
[24] B. A. Strukov and A. P. Levanyuk, *Ferroelectric Phenomena in Crystals* (Springer, Heidelberg, 1998), p. 303.
[25] M. D. Glinchuk and A. N. Morozovskaya, Phys. Status Solidi B **238**, 81 (2003).
[26] Z. Zhao, V. Buscaglia, M. Viviani, M. T. Buscaglia, L. Mitoseriu, A. Testino, M. Nygren, M. Johnsson, and P. Nanni, Phys. Rev. B **70**, 024107 (2004).
[27] E. Erdem, H.-Ch. Semmelhack, R. Bottcher, H. Rumpf, J. Banys, A. Matthes, H.-J. Glasel, D. Hirsch, and E. Hartmann, J. Phys.: Condens. Matter **18**, 3861 (2006).
[28] A. N. Morozovska, M. D. Glinchuk, and E. A. Eliseev, Phys. Rev. B **76**, 014102 (2007).
[29] J. X. Zhang, Y. L. Li, Y. Wang, Z. K. Liu, L. Q. Chen, Y. H. Chu, F. Zavaliche, and R. Ramesh, J. Appl. Phys. **101**, 114105 (2007).
[30] M. J. Haun, E. Furman, S. J. Jang, and L. E. Cross, Ferroelectrics **99**, 63 (1989).
[31] F. Jona and G. Shirane, *Ferroelectric Crystals* (Pergamon, Oxford, 1962).
[32] J. A. Lopez-Perez, M. A. Lopez Quinterla, J. Mira, J. Rivas, and S. W. Charles, J. Phys. Chem. B **101**, 8045 (1997).
[33] B. Jaffe, W. R. Cook, and H. Jaffe, *Piezoelectric Ceramics* (Academic, London, 1971).
[34] D. J. Hudson, in *Statistics*, Lectures on Elementary Statistics and Probability (CERN, Geneva, 1964); B. R. Martin, *Statistics for Physicists* (Academic, London, 1971).